ISSN 0036-0244, Russian Journal of Physical Chemistry A, 2020, Vol. 94, No. 9, pp. 1887–1901. © Pleiades Publishing, Ltd., 2020.

STRUCTURE OF MATTER AND QUANTUM CHEMISTRY

Thermodynamic and IR Spectral Study of Metal Cations–Anthocyanin Chelation: Mechanism of Formation of Pigments

Fatemeh Mollaamin[a,]* and Majid Monajjemi[a]

[a] *Department of Chemical Engineering, Central Tehran Branch, Islamic Azad University, Tehran, Iran*

* *e-mail: smollaamin@gmail.com*

Received September 3, 2019; revised December 26, 2019; accepted January 17, 2020

Abstract—Metal ions chelation of some anthocyanins [ACN-$Al^{3+}/Ga^{3+}/Cr^{3+}/Fe^{3+}/Mg^{2+}$] chelation in aqueous medium were investigated to discover the color fluctuation of different derivatives of these compounds at low pH. Chelation of M^{n+} by ACN also improved the color expression range of ACN in more different pH environments. In this verdict, it has been studied the metal ions diffusing of deprotonating for the ACN B-ring of cyanidin (Cy), delphinidin (Dp), and petunidin (Pt) in vacuum and water media, transforming flavylium cations to the blue quinonoidal bases at lower pH using the infrared method though pursuing Beer–Lambert law for finding the physical and chemical properties of frequency, intensity, and absorbance of the compounds, respectively. In this wok, it has been illustrated that the important factor for increasing the absorbance in a positive non-linear fashion due to deviating from the Beer–Lambert law is the self-association of anthocyanins of Cy, Dp, and Pt anthocyanins. The difference of ΔH_R among [ACN-$Al^{3+}/Ga^{3+}/Cr^{3+}/Fe^{3+}/Mg^{2+}$] chelation complexes has been discussed the double bonds and carbonyl groups through the chelation of B ring for Cy, Dp, and Pt anthocyanins in vacuum and water media that explains the stability and color of [ACN-$Al^{3+}/Ga^{3+}/Cr^{3+}/Fe^{3+}/Mg^{2+}$] chelation of Cy, Dp, and Pt pigments in a weak acidic condition. The ACNs of Cy, Dp, and Pt with highest chelate in the active part of these structures by metal ions of $Al^{3+}/Ga^{3+}/Cr^{3+}/Fe^{3+}/Mg^{2+}$ produce a variety range of colors under acidic pH; as divalent Mg^{2+} has shown various physicochemical properties considering its optimized geometry optimization as the bond length of O⋯Mg^{2+} ≈1.9 Å and the bond angle of O⋯Mg^{2+}⋯O ≈112° while it has been indicated the bond length of O⋯M^{3+} ≈1.8 Å and bond angle of O⋯M^{3+}⋯O ≈120° for trivalent metal cations of $Al^{3+}/Ga^{3+}/Cr^{3+}/Fe^{3+}$ with more electron rich metal ions caused shifts and hue changes in the stability of color and structure. Moreover, we have found that [ACN-$Al^{3+}/Ga^{3+}/Cr^{3+}/Fe^{3+}/Mg^{2+}$] chelation is dependent on the position of active cites of labeled oxygen atoms and cations in these structures which transfer the charge of electrons in aromatic cyclic chains because of water polar medium in contrast to vacuum. The spin density and partial charges have been obtained by fitting the electrostatic potential to fixed charge of O^+_{17}, O^+_{16}, and O^+_7 cations for Cy-M^{n+} (31), Dp-M^{n+} (32), and Pt-M^{n+} (35), respectively based on the electrophilic groups of Cy, Dp, and Pt anthocyanin pigments which unravel the activity and the stability of these compounds in the natural products.

Keywords: [ACN-$Al^{3+}/Ga^{3+}/Cr^{3+}/Fe^{3+}/Mg^{2+}$] chelation, anthocyanin, anthocyanin–metal chelate, metalloanthocyanin, IR, Beer–Lambert law, Cy, Dp, Pt, vacuum, water

DOI: 10.1134/S0036024420090204

INTRODUCTION

The structures of anthocyanin water-soluble and polar derivatives which have a wide membrane bound vesicle in a cell's cytoplasm can be seen in different colors in an expanded range of colors such as red, purple, blue or black [1–3] (Scheme 1a). The aromatic cyclic group of anthocyanins are a part of fundamental compounds as flavonoids synthesized via the phenylpropanoid pathway which are discovered in roots, stems, leaves, flowers, and fruits.

The proportion of the most common anthocyanidins in fruits and vegetables including cyanidin, delphinidin, pelargonidin, peonidin, malvidin, and petunidin is 50, 12, 12, 12, 7, and 7%, respectively [4].

In nature, cyanidin in berries is a reddish-purple major pigment and other red-colored vegetables such as red sweet potato and purple corn [5, 6]. Delphinidin has a chemical characteristic similar to most of the anthocyanidins which appears as a blue-reddish or purple pigment in the plant like the blue hue of flowers which is due to the delphinidin pigment [7]. But pelar-

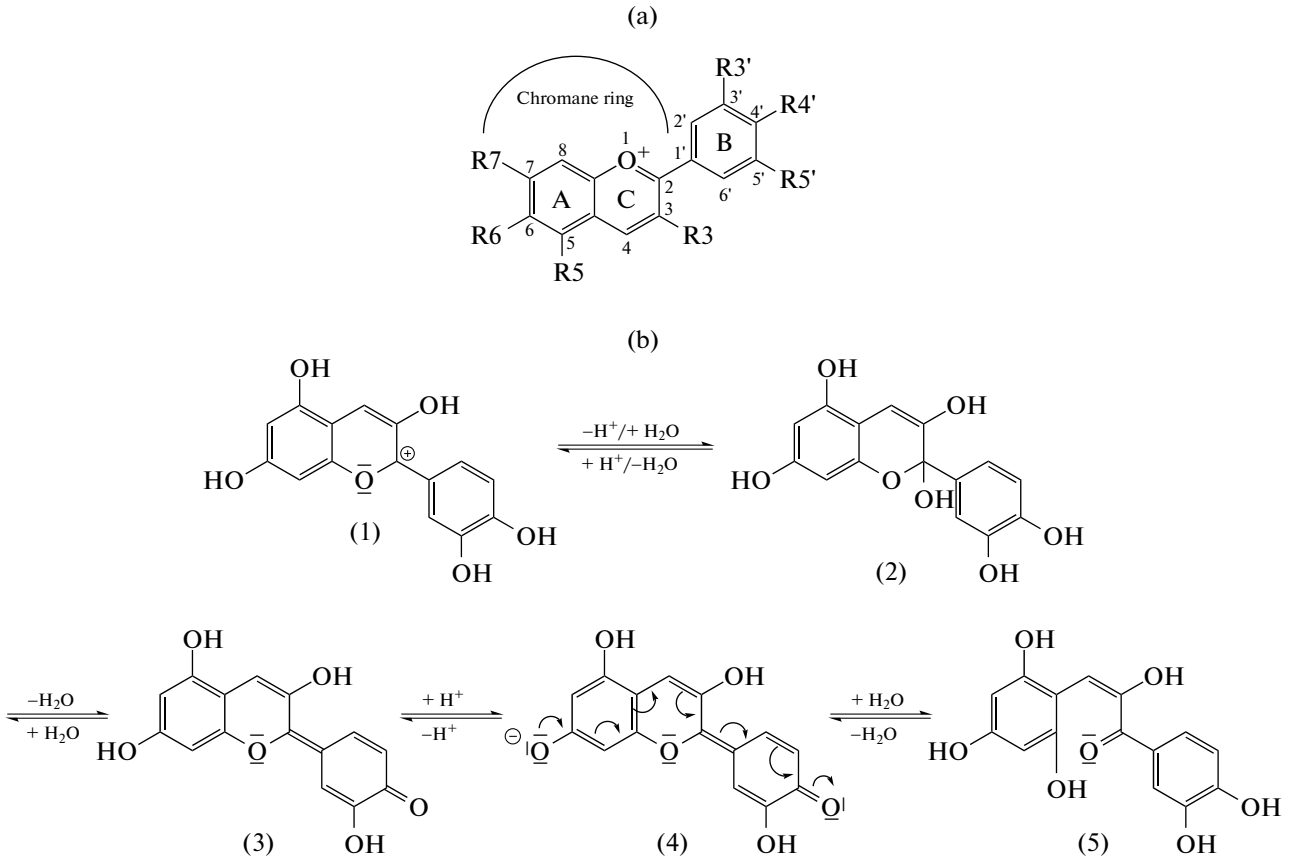

Scheme 1. Basic anthocyanin structure [29] (a) and the anthocyanidin pigments reveal a variety of molecular transformations with the pH changes, and generating different colors (b); (1) flavylium cation, pH >3 red, (2) carbonyl pseudo base (pH 4–5 colorless), (3) anhydrobase (pH 6–7 violet), (4) anhydrobase anion (pH 7–8 blue), (5) chalcone (pH >8 yellow).

gonidin is different from most of the anthocyanidins as a red-colored pigment [8]. Besides, pelargonidin donates an orange hue to flowers and red to some of the fruits and berries [9, 10].

In acidic media, anthocyanin appears as a red pigment while blue pigment anthocyanin appears in alkaline media. Anthocyanin is considered as one of the flavonoids with a positive charge at the oxygen atom of the C-ring (Scheme 1a). The studies on the natural antioxidnats are significant for nutrition science and public health [11–14].

Fruits and vegetables contain antioxidants like vitamins C and E, carotenoids and flavonoids and their characteristics including molecular weight, dimensional conformation, biochemical and physical characteristics of these compounds conduct them to react with different points in many live organisms [15–17]. The compounds of anthocyanin pigments are a big family of polyphenolic molecules as flavonoids that are founded by plants as the part of their secondary metabolism. Flavonoids are divided into different subclasses based on their chemical characteristics and share a popular carbon basis called flavylium ion chain with different rings [18, 19].

The glycosylated anthocyanidin groups which are linked to the skeleton of anthocyanin have the highest common type of pigments in plants. So, it can be found a variety of anthocyanins due to complex glycosylation models over some aglycones. These compounds are largely colored at weak acidic condition, low pH, through the eight conjugated double bonds exhibiting a positive charge of the structure that show various colors due to various substitutions in the aromatic cyclic chains [20–24]. Physicochemical properties of anthocyanin structures are affected by the nature of substituents due to changing the size, polarity and solubility in water toward an expanded range of compounds in nature [25]. It is important how the plants arrange the structure or how chemistry of the anthocyanins produces an expanded range of colors often in the visible spectrum [26]. Moreover, for indicating the color and stability of anthocyanins through the chemical and other photochemical properties, several new anthocyanin-inspired dyes and pigments have been prepared for applying in cosmetics or foods with pleasant colors and stability in comparison to the color and stability of natural anthocyanins [27]. The scientists have explained that the color of natural

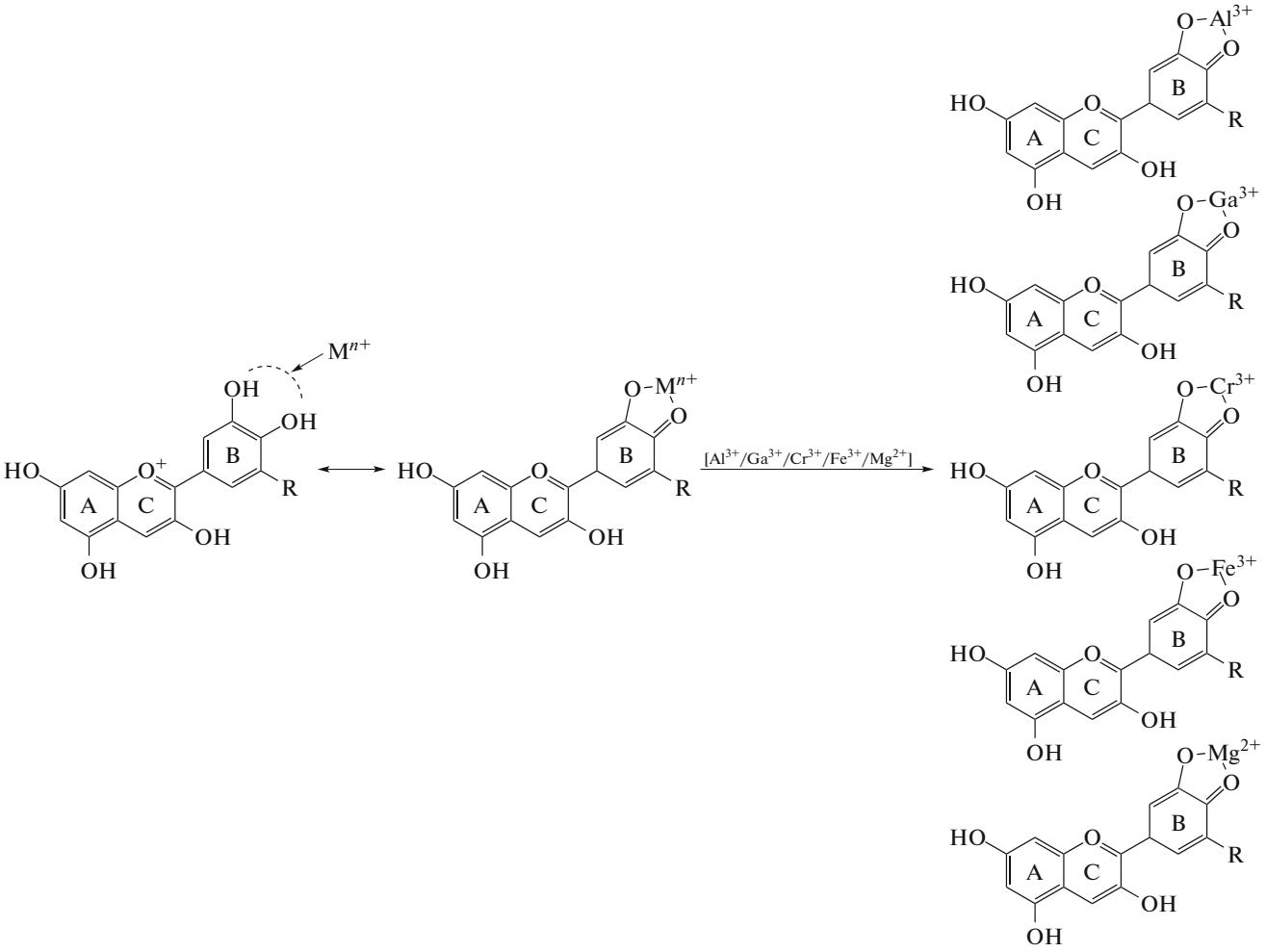

Scheme 2. Proposed mechanism of ACN-metal cation chelation of $Al^{3+}/Ga^{3+}/Cr^{3+}/Fe^{3+}/Mg^{2+}$ through the B ring for three anthocyanins of cyanidin, delphinidin, and petunidin [31].

anthocyanins is sensitive to concentration of H^+ in the solution (weak acidic media are appropriate). Around pH 3, changing the color generates the colored anthocyanin cation, AH^+, which alters into colorless or near-colorless samples (Scheme 1b) [28].

Glińska and his coworkers have illustrated the decrease of potential toxic effects of ACNs through separating M^{n+} chelation of these compounds [30]. Due to metal cation chelation and expressing purple blue colors, the molecule of anthocyanin must tolerate at least two free hydroxyl groups on the B ring. When the cation approaches the anthocyanins, it plays a role to compete with the hydrogen ions for the binding sites (Scheme 2) [31].

The chelation of $Al^{3+}/Ga^{3+}/Cr^{3+}/Fe^{3+}/Mg^{2+}$ by Cy, Dp, and Pt has been more extensively studied due to its relationship with the blue coloration of hydrangea floral compounds. Relatively, stable complexes between Dp and Al^{3+} have been investigated to form acidified ethanol and a wide pH range [31]. In these structures, color expression of the Dp began red becoming violet and then blue as pH and ACN concentration were maintained, but the Al^{3+} content increased. Chelation of Al^{3+} with Cy has been identified to develop in aqueous samples, pH 2–5 which indicate violet colorations [32].

Buchweitz and his co-workers compared the stability of Al^{3+} chelates of Dp-3-rutinoside in American eggplant to that of acylated Cy glycosides, red cabbage, as literature is limited about stability of acylated ACN metal chelates. They explained that ACN metal complexes are stronger to heat treatment rather than light exposure. Degradation of Dp-Al chelates seems jointed to concentration with rate decreasing of time, in agreement with recent researches [33].

In the recent researches, it has been approved that Al^{3+} in metalloanthocyanins is capable of inducing blue color development with Dp, having a pyrogallol moiety on the B ring, but it is not enough to lead to blue colors with Cy derivatives [34]. Therefore, a the-

Table 1. Optimized geometry with m062x/cc-pvdz pseudo=lanl2 for various [ACN-Al^{3+}/Ga^{3+}/Cr^{3+}/Fe^{3+}/Mg^{2+}] chelation extracted of Fig. 1 (l is bond length, α is bond angle)

Cyanidin–metal ion chelate	Bond	l, Å	Bond	α, deg
Cy-Mg^{2+}	O(10)⋯Mg^{2+}(31)	1.997	O(10)⋯Mg^{2+}(31)⋯O(27)	112.833
	Mg^{2+}(31)⋯O(27)	1.996		
Cy-Al^{3+}/Cr^{3+}	O(10)⋯Al^{3+}/Cr^{3+}(31)	1.8232	O(10)⋯Al^{3+}/Cr^{3+}(31)⋯O(27)	121.202
	Al^{3+}/Cr^{3+}(31)⋯O(27)	1.8231		
Cy-Fe^{3+}	O(9)⋯Fe^{3+}(32)	1.8137	O(10)⋯Fe^{3+}(31)⋯O(27)	121.658
	Fe^{3+}(32)⋯O(26)	1.8136		
Cy-Ga^{3+}	O(10)⋯Ga^{3+}(31)	1.8987	O(10)⋯Ga^{3+}(31)⋯O(27)	117.55
	Ga^{3+}(31)⋯O(27)	1.8995		

oretical study of the linkage between the electronic and chemical structure of Al^{3+}/Ga^{3+}/Cr^{3+}/Fe^{3+}/Mg^{2+} by Cy, Dp, and Pt and their stability has been followed using theoretical and computational methods in vacuum and water media at 300 K based considering Beer–Lambert law for discovering different usages of these structures such as coloring agents in pharmaceutical products and foods. Moreover, it has been illustrated the structural properties of [Al^{3+}/Ga^{3+}/Cr^{3+}/Fe^{3+}/Mg^{2+}] chelation by quantum chemical methodologies as the computational design and the simulated class to estimate the physicochemical characteristics of these chelated pigments with metal ions through conserving their stability and color tide.

BACKGROUND OF CHELATION

The chelation of anthocyanins of cyanidin, delphinidin and petunidin with Al^{3+}/Ga^{3+}/Cr^{3+}/Fe^{3+}/Mg^{2+} has been studied in this investigation by forming relatively stable complexes in the weak acidified medium with a different pH range. Thus, a series of quantum theoretical approaches has been done for finding the optimized coordination of [ACN-Al^{3+}/Ga^{3+}/Cr^{3+}/Fe^{3+}/Mg^{2+}] chelation with IR computations and following the Beer–Lambert law using Gaussian09 program package [35]. It has been declared that polarization functions into the applied basis set in the computation always introduce us an important achievement on the modeling and simulation theoretical levels. Normal mode accomplishment is the verdict of harmonic potential wells by analytic methods which maintain the motion of all atoms at the same time in the vibration time scale leading to a natural explanation of molecular vibrations [36–41].

First, optimized geometry coordination of [cyanidin-Al^{3+}/Ga^{3+}/Cr^{3+}/Fe^{3+}/Mg^{2+}] chelation complexes (Fig. 1) through their B ring in vacuum and water media at 300 K have been evaluated in Table 1.

Besides, charge electron transfer and thermodynamic properties of [ACN-Al^{3+}/Ga^{3+}/Cr^{3+}/Fe^{3+}/Mg^{2+}] chelation through their B ring in vacuum and water media at 300 K have been evaluated and compared to each other by different concentration of H^+ in a simulated solvent model (Fig. 1).

In this work, the data has been achieved from thermodynamic parameters of ΔG, ΔH, and ΔS for the solute–solvent model of [ACN-Al^{3+}/Ga^{3+}/Cr^{3+}/Fe^{3+}/Mg^{2+}] chelation solved in water solvent at 300 K compared to vacuum medium were analyzes. Therefore, for accomplishing a stable structure of [ACN-Al^{3+}/Ga^{3+}/Cr^{3+}/Fe^{3+}/Mg^{2+}] chelation of Cy, Dp, and Pt pigments, geometry optimization plus frequency calculations were done; the frequency and intensity of the vibrational modes were calculated with the QM theoretical method, and the principal vibrational modes were analyzed by their changes of Gibbs free energy in water compared to water medium at 300 K. Thermochemistry analysis follows the frequency and normal mode data. The zero-point energy output in Gaussian-09 has been expanded and corrected as: thermal correction to energy, thermal correction to enthalpy and thermal correction to the Gibbs free. In addition the total energies can be calculated as: sum of electronic and zero point energies, sum of electronic and thermal energies, sum of electronic and thermal enthalpies and sum of electronic and thermal Gibbs free energies.

The theoretical calculations were done at various levels of theory to gain the more accurate equilibrium geometrical results and IR spectral data for each of the identified compounds. It is supposed that an additional diffuse and polarization functions into the basis set applied in the computation conduct us to the magnificent progress on the results of theoretical methods. The simulation indicates the approaches which produce a common template of a model at a special tem-

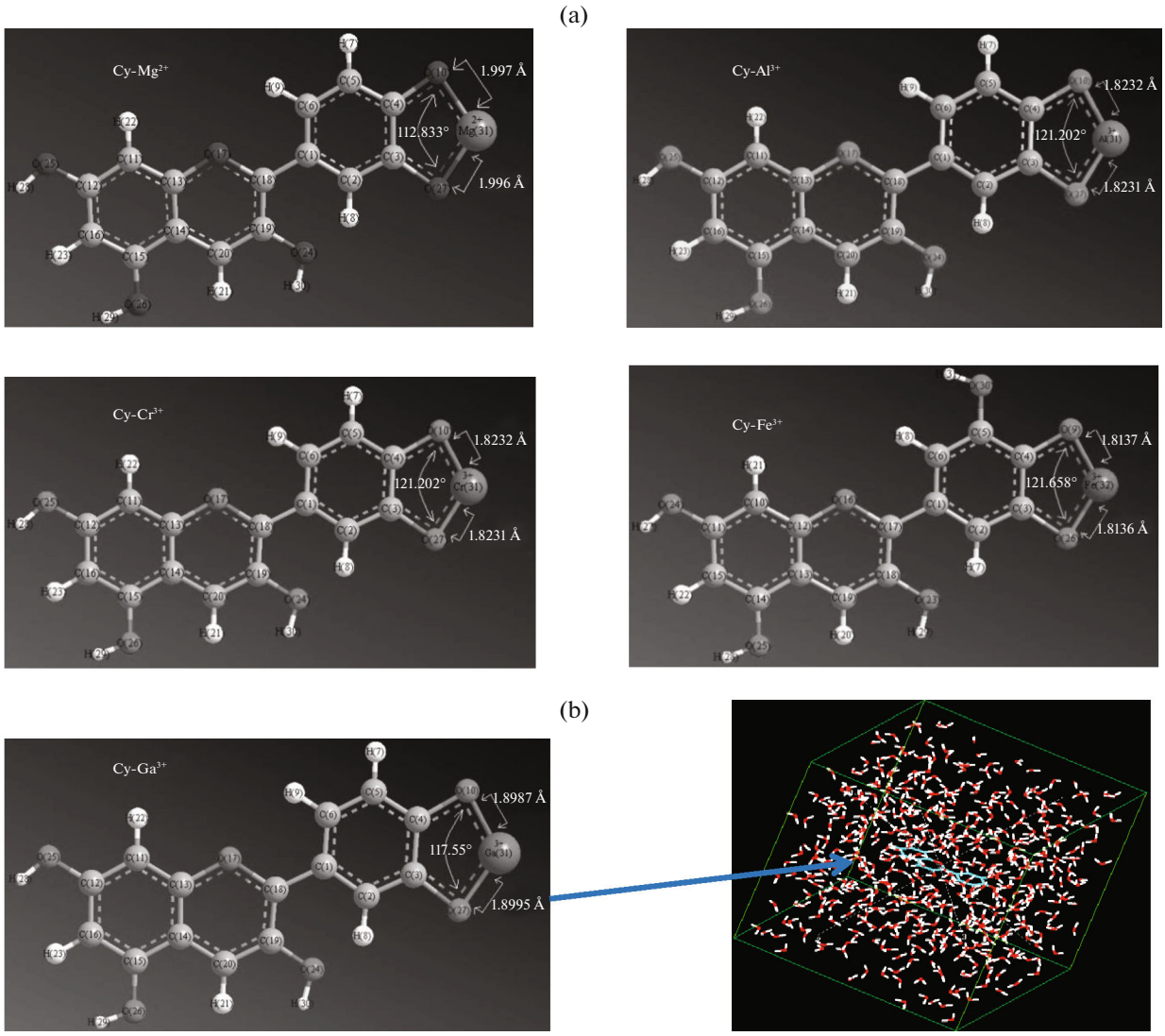

Fig. 1. (Color online) (a) The schematics of ab initio optimized coordination [cyanidin-Al^{3+}/Ga^{3+}/Cr^{3+}/Fe^{3+}/Mg^{2+}] through representing the bond length of O⋯M^{n+} and bond angle of O⋯M^{n+}⋯O calculated by m062x/cc-pvdz pseudo=lanl2. (b) Solvation optimized with QM/MM model of anthocyanins' family inside 500 water molecules as solvent, including 3 levels of m06-HF for the high (H) layer, Pm3MM semi empirical for the medium and Monte Carlo for low layers at 300 K.

perature by computing all physicochemical properties among the partition function [37].

COMPUTATIONAL DETAILS

Each part of the systems including Cy–Mg^{2+}, Cy–Al^{3+}/Cr^{3+}, Cy–Fe^{3+}, and Cy–Ga^{3+} have been optimized using ab inito via density functional theory including ECP calculations with lanl1, lanl2 basis sets and pseudo key due to the metals. In addition those systems have been evaluated via QM/MM approach through an ONIOM method. In our study, differences of force fields are debated through comparing density and energies with OPLS and AMBER via Monte Carlo optimization. In addition, a Hyper-Chem professional release 7.01 program has been applied for some additional keywords such as PM3MM, PM6 (pseudo=lanl2).

The DFT with the van der Waals densities functional were investigated for modeling of solvent–compounds interaction. All optimization of solvent effects were done by Gaussian-09. The accurate calculations performed using m062x, m06-L, and m06 for cyanidin–metal ion chelate interaction. The m062x, m06-L, and m06-HF methods have a suitable correspondence in non-bonded calculations between these compounds and solvents. The ONIOM levels have been applied through 3 levels of high (H), medium (M), and low (L) calculations which DFT methods were used for the high (H) layer and the semi empirical

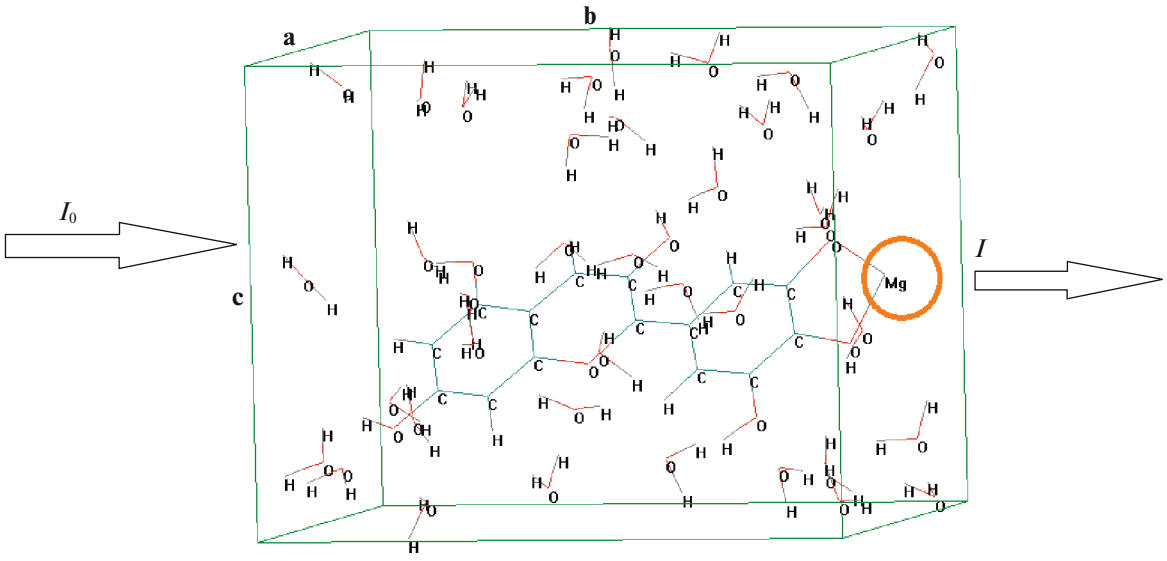

Scheme 3. (Color online) The relation of light intensity in the Beer–Lambert law with concentration aspect of metal ion chelation of anthocyanin's family like CAN–Mg^{3+} in water.

method of pm6 and Pm3MM was used for the medium and finally Monte Carlo for low layers, respectively.

The Polarizable continuum model, PCM, is the most popular SCRF model based on apparent surface charges expanding to discuss non-electrostatic impacts using scaled point theory [42, 43].

Rinaldi and Rivail developed the most common levels of the SCRF method of multiple expansions with an algorithm based on the use of a strict multipolar expansion up to the 7th order by Frisch that is currently available at both semi-empirical and ab initio levels of theory. Onsager and Kirkwood have arranged an intention for various continuum solvation examples of a multiple expansion, MPE, of the solute charge distribution [44–46]. Then, Wiberg et al. improved Onsager-SCRF for the Gaussian program [47, 48].

Solvation is illustrated in terms of a dipole moment with an iterative path of quantum mechanics calculations on the structure. The perspective of Onsager-SCRF was one to directly apply almost all of the computational characteristics of Gaussian program. The dielectric continuum models like the self-consistent reaction field approach are efficient in applying account the long range of solute–solvent electrostatic interactions and the effect of solvent polarization. Another theoretical level is combination of molecular mechanics (MM) solvent molecule with quantum mechanics level (QM) for electronic structure of the solute molecule named QM/MM which can modify deficiency of the dielectric continuum model [49, 50].

Absorbance is a direct measure of how much light is absorbed by our samples in this work. As the absorbance can take on values between 0 (at 100% transmittance) and about 2.0 (at 1% transmittance); thus large values of absorbance are associated with very little light passing entirely through the sample and small values of absorbance are associated with most of the light passing entirely through the samples. We could imagine two interesting situations. First one, if we pass a beam of light of the appropriate wavelength through a fairly dilute solution, second, we could imagine that the photons will encounter a small number of the absorbing by the metal ions of chemical species such as Mg^{2+}, Al^{3+}, Cr^{3+}, Fe^{3+}, and Ga^{3+}, so we might expect a high % transmittance and a low absorbance. Alternatively, if we pass the same beam of light through a highly concentrated solution, we could imagine that the photons will encounter a large number of the absorbing chemical species including Cy–Mg^{2+}, Cy–Al^{3+}/Cr^{3+}, Cy–Fe^{3+}, and Cy–Ga^{3+}.

In this work, light goes through a number of molecules as a system (refers to Scheme 1b), the anthocyanidin pigments reveal a variety of molecular transformations with the pH changes, and generating different colors; (1) flavylium cation (pH >3 red), (2) carbonyl pseudo base (pH 4–5 colorless), (3) an hydro base (pH 6–7 violet), (4) anhydro base anion (pH 7–8 blue), (5) chalcone (pH >8 yellow)], therefore $\frac{I_0}{I_1} = \frac{I_2}{I_3} + \frac{I_3}{I_4} + \frac{I_4}{I_5} = n$. This qualitative relationship is described by the following function for light intensity: $I_i = I_0 n^{-i}$ or $I_i = 10^{-i \log_n^{10}}$ where i is the number of species in mechanism. The last expression may be gener-

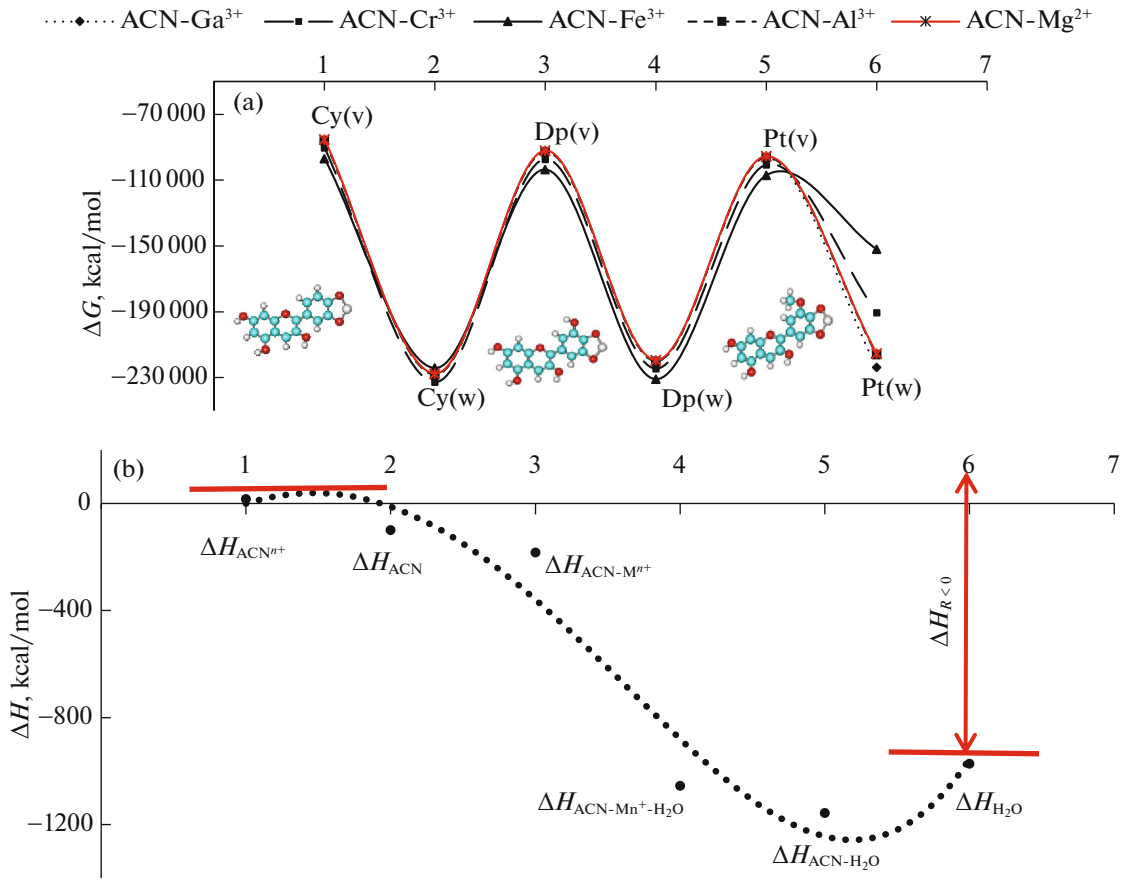

Fig. 2. (Color online) (a) Changes of Gibbs free energy (ΔG, kcal/mol) of [ACN-Al^{3+}/Ga^{3+}/Cr^{3+}/Fe^{3+}/Mg^{2+}] chelation in vacuum (v) and water (w) media at 300 K; (b) changes of enthalpy of reaction (ΔH_R) for formation of [ACN-Al^{3+}/Ga^{3+}/Cr^{3+}/Fe^{3+} /Mg^{2+}]-chelation complexes in water medium.

alized for any systems with light path-length (l): $I = I_0 10^{-kl}$, where k is a coefficient which depends on concentration, c, and molar absorptivity, ε: consequently, $k = \varepsilon c$ (Scheme 3).

RESULTS AND DISCUSSION

In this project, three anthocyanin pigments of cyanidin, delphinidin, and petunidin have been estimated using theoretical methods to measure the effect of metal chelation of different plants including factorial excess of Al^{3+}/Ga^{3+}/Cr^{3+}/Fe^{3+}/Mg^{2+} in different pH and evaluated by IR spectroscopy using Gaussian09 in vacuum and water media at 300 K (Fig. 1).

The thermodynamic properties of ΔG, ΔH, ΔS, electronic energy and core–core interaction, frequency spectrums, anthocyanin concentration, and pH determined final color and intensity (Table 2 and Figs. 2a, 2b) [35].

The difference of ΔH_R among [ACN-Al^{3+}/Ga^{3+}/Cr^{3+}/Fe^{3+}/Mg^{2+}] chelation complexes (Fig. 2b) has been unraveled due to double bonds and carbonyl groups through the chelation of B ring for Cy, Dp and Pt anthocyanins in vacuum and water media that illustrates the stability and color of [ACN-Al^{3+}/Ga^{3+}/Cr^{3+}/Fe^{3+}/Mg^{2+}] chelation of Cy, Dp, and Pt pigments in a weak acidic condition (Fig. 1). The highest chelate stability with different ACNs indicates that ACN-metal chelation can produce a variety range of colors under acidic pH with efficiency for food consume. The results of ΔH_R for formation of [Cy, Dp, Pt-Al^{3+}/Ga^{3+}/Cr^{3+}/Fe^{3+}/Mg^{2+}] chelation complexes have been extracted by Fig. 2b and data of Tables 2 and 3.

In the present project, Beer–Lambert law has been used for optimized compounds of [Cy, Dp, Pt-Al^{3+}/Ga^{3+}/Cr^{3+}/Fe^{3+}/Mg^{2+}] chelation to demonstrate the absorbance of assigned molecules toward showing the stabilization and a range of color due to their electronic structures in H_2O media with different

Table 2. Thermodynamic properties of $Al^{3+}/Ga^{3+}/Cr^{3+}/Fe^{3+}/Mg^{2+}$ chelation for Cy, Dp, Pt pigments in vacuum (v) and water (w) media at 300 K, calculated by m062x/cc-pvdz pseudo=lanl2

Chelation	ΔG, kcal/mol	ΔH, kcal/mol	ΔS, kcal//(K mol)	$E_{electronic}$, kcal/mol	$E_{core\text{-}core}$, kcal/mol
Cy-Al^{3+}(v)	-8.5857×10^4	−83.2924972	285.9145815	-5.4036×10^5	4.5451×10^5
Cy-Al^{3+}(w)	-2.2817×10^5	−1055.370675	757.0659268	-2.2226×10^6	1.9945×10^6
Dp-Al^{3+}(v)	-9.2631×10^4	−125.1253726	308.3548311	-5.9126×10^5	4.9863×10^5
Dp-Al^{3+}(w)	-2.1997×10^5	−1002.58787	729.9112981	-2.0720×10^6	1.8521×10^6
Pt-Al^{3+}(v)	-9.6061×10^4	−112.0089867	319.8319042	-6.4155×10^5	5.4548×10^5
Pt-Al^{3+}(w)	-2.1592×10^5	−940.4675265	716.5909319	-2.0674×10^6	1.8515×10^6
Cy-Ga^{3+}(v)	-8.6017×10^4	−16.3560	286.6719	-5.4090×10^5	4.5488×10^5
Cy-Ga^{3+}(w)	-2.2833×10^5	−1055.3706	757.5847	-2.2238×10^6	1.9954×10^6
Dp-Ga^{3+}(v)	-9.2788×10^4	−55.2946	309.1121	-5.9184×10^5	4.9906×10^5
Dp-Ga^{3+}(w)	-2.2022×10^5	−1026.1415	730.6686	-2.0722×10^6	1.8520×10^6
Pt-Ga^{3+}(v)	-9.6272×10^4	−96.1243	320.5892	-6.4222×10^5	5.4594×10^5
Pt-Ga^{3+}(w)	-2.2366×10^5	−1023.9666	742.1457	-2.1879×10^6	1.9642×10^6
Cy-Cr^{3+}(v)	-9.0353×10^4	−9.0901	301.1496	-5.6780×10^5	4.7744×10^5
Cy-Cr^{3+}(w)	-2.3275×10^5	−1065.9298	772.3010	-2.2732×10^6	2.0405×10^6
Dp-Cr^{3+}(v)	-9.7191×10^4	−114.2305	323.5899	-6.2009×10^5	5.2290×10^5
Dp-Cr^{3+}(w)	-2.2456×10^5	−1021.4739	745.1463	-2.1219×10^6	1.8973×10^6
Pt-Cr^{3+}(v)	-1.0060×10^4	−78.2840	335.0669	-6.7134×10^5	5.7074×10^5
Pt-Cr^{3+}(w)	-1.9050×10^5	−709.7708	632.6362	-1.7197×10^6	1.52927×10^6
Cy-Fe^{3+}(v)	-9.6847×10^4	−133.8576	322.3788	-5.8856×10^5	4.9171×10^5
Cy-Fe^{3+}(w)	-2.2420×10^5	−1022.2549	743.9352	-2.1020×10^6	1.8778×10^6
Dp-Fe^{3+}(v)	-1.0352×10^4	−78.5366	344.8190	-6.4155×10^5	5.3802×10^5
Dp-Fe^{3+}(w)	-2.3100×10^5	−1090.2568	766.3755	-2.1573×10^6	1.9263×10^6
Pt-Fe^{3+}(v)	-1.0705×10^4	−160.3138	356.2961	-6.9356×10^5	5.8651×10^5
Pt-Fe^{3+}(w)	-1.5199×10^5	−470.1788	505.0807	-1.1946×10^6	1.0426×10^6
Cy-Mg^{2+}(v)	-8.5215×10^4	−45.6907	283.8974	-5.3287×10^5	4.4765×10^5
Cy-Mg^{2+}(w)	-2.2760×10^5	−1083.7536	755.0487	-2.2076×10^6	1.9800×10^6
Dp-Mg^{2+}(v)	-9.1986×10^4	−84.9301	306.3376	-5.8342×10^5	4.9143×10^5
Dp-Mg^{2+}(w)	-2.1940×10^5	−1033.6429	727.8941	-2.0569×10^6	1.8375×10^6
Pt-Mg^{2+}(v)	-9.5415×10^4	−71.1751	317.8147	-6.3344×10^5	5.3802×10^5
Pt-Mg^{2+}(w)	-2.1534×10^5	−970.6360	714.5737	-2.0521×10^6	1.8367×10^6

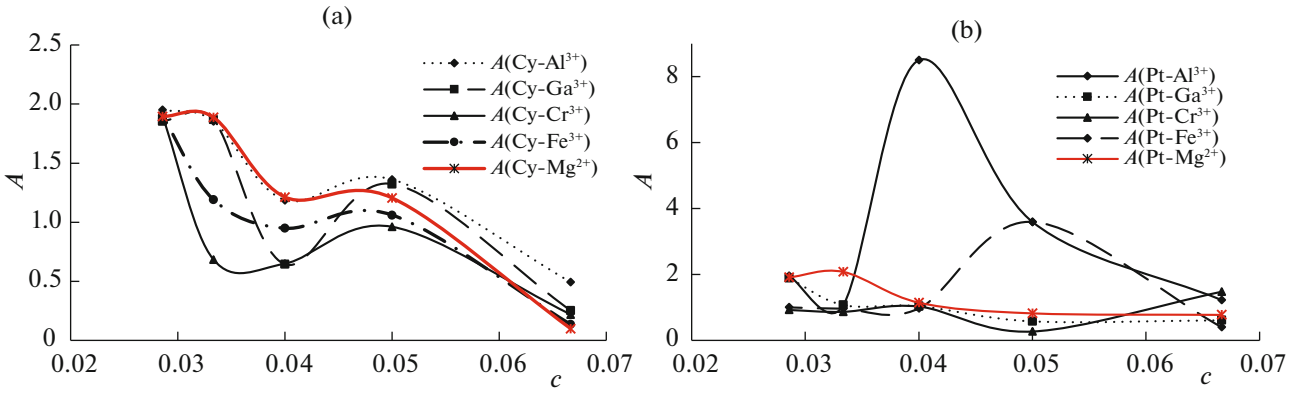

Fig. 3. (Color online) Changes of absorbance (A) versus concentration (c) through Beer–Lambert law for (a) [Cy-Al^{3+}/Ga^{3+}/Cr^{3+}/Fe^{3+}/Mg^{2+}] chelation and (b) [Pt-Al^{3+}/Ga^{3+}/Cr^{3+}/Fe^{3+}] chelation in the weak acidic media by different concentrations of H^+ at 300 K.

concentrations of H^+ (Table 4). The absorbance (A) of the anthocyanins—Al^{3+}/Ga^{3+}/Cr^{3+}/Fe^{3+}/Mg^{2+} ion chelation of Cy, Dp, and Pt pigments in H_2O periodic box of a simulated model has been calculated through the Beer–Lambert law which directly depends on concentration (c, mol/L) of H^+. The results have been shown in Table 4 based on basic equations of $A = \log(I_0/I) = \varepsilon lc$, where A is the absorbance; I is intensity of current; ε is molar absorptivity coefficient; and c is concentration of solution. Basically, the increase in absorbance continued to rise with increasing and decreasing of frequency (F) for anthocyanin-metal cation chelation of Cy–Al^{3+} and Pt–Al^{3+} in higher pH, respectively (Figs. 3a, 3b).

These decreases in absorbance could be related to decreased solubility of the CAN–M^{n+} complexes which are resulted in precipitation of some complexes. In neutral or alkaline pH, hyper-chromic effects were found to be highest with much lower M^{n+} levels; they were largest in higher pH with M^{n+} and [ACN], respectively, and were pursued by absorbance decreases (Figs. 3a, 3b).The large increases in absorbance could be treated to convert as the colorless forms of ACN to those which absorb and reflect visible light as well as the M^{n+} induced linked to ACN compounds (Figs. 3a, 3b).

There is a high tendency to the absorbance of Cy, Dp, and Pt with Mg^{2+} added, but the changes were of small magnitude by playing a role in organizing ACN into supramolecular assembly similar to the role of Mg^{2+} which plays in metalloanthocyanins formation [34]. Mg^{2+} is the only divalent metal cation used in this work which is a crucial M^{n+} to life system and usually linked to ACN in plant systems lacking any electrons in d orbitals, and it is able to produce some metalloanthocyanins with the unfilled d or f orbitals [51]. Mg^{2+} was found to do function in the stereochemical configurations of Cy, Dp, and Pt anthocyanins (Fig. 1). For discovering the impacts of Al^{3+} salt on food origin, ACN were measured with the goal to better understanding blue color development of metallo-ACN.

In calculations, Al^{3+} was identified to displace Mg^{2+} in ACN-Mg^{2+} complexes, Cy based, and produces more stable complexes [52]. This M^{n+} has also even been estimated as a key to evaluate Cy, Dp, and Pt in ACN extracts from edible sources [53]. Similar to Mg^{2+}, Al^{3+} also lacks electrons in d orbitals but is trivalent when ionized.

In all pH, the frequency, intensity, absorbance, and thermodynamics properties (Table 4) of ACN-chela-

Table 3. The difference of ΔH_R through formation of [ACN-Al^{3+}/Ga^{3+}/Cr^{3+}/Fe^{3+}/Mg^{2+}-chelation] complexes (ACN–M^{n+}–H_2O), kcal/mol

ACN	$M^{n+} = Al^{3+}$	$M^{n+} = Ga^{3+}$	$M^{n+} = Cr^{3+}$	$M^{n+} = Fe^{3+}$	$M^{n+} = Mg^{2+}$
Cy	−1072.0889	−939.0038	−1056.8397	−788.3865	154.3308
Dp	−894.7528	−828.4312	−935.4285	−869.3045	199.9012
Pt	−1094.7862	−1151.5006	−1128.5112	−1046.4814	−178.9623

Table 4. Calculated absorbance (A), frequency (f), and dipole moment (μ) of anthocyanin-metal chelation of Cy, Dp, and Pt in various pH

pH	A	f, 1/cm	μ, D	A	f, 1/cm	μ, D	A	f, 1/cm	μ, D	A	f, 1/cm	μ, D	A	f, 1/cm	μ, D
	Cy-Al^{3+}			Cy-Ga^{3+}			Cy-Cr^{3+}			Cy-Fe^{3+}			Cy-Mg^{2+}		
1.1761	0.2533	3924.86	18.655	0.2533	3924.86	18.655	0.2197	3926.3	9.94	0.1354	3924.71	7.384	0.100	3922.7	3.047
1.3010	1.3242	3925.22	16.739	1.3242	3925.22	16.739	0.9616	3931.09	8.391	1.0612	3926.28	5.914	1.2056	3927.39	3.24
1.3979	0.6445	3926.23	16.351	0.6445	3926.23	16.351	0.6494	3926.2	10.313	0.9492	3926.28	7.149	1.2132	3927.39	1.532
1.4771	1.8690	4008.35	13.82	1.8690	4008.35	13.82	0.6843	3926.21	8.592	1.1914	3928.35	4.695	1.8876	4014.5	5.276
1.5440	1.8553	4007.68	6.687	1.8553	4007.68	6.687	1.8981	4009.28	9.588	1.9019	4012.01	6.471	1.8952	4012.12	3.911
	Dp-Al^{3+}			Dp-Ga^{3+}			Dp-Cr^{3+}			Dp-Fe^{3+}			Dp-Mg^{2+}		
1.1761	3.5939	3925.8	1617.192	0.4210	3925.41	18.783	0.8937	3933.41	9.042	0.8899	3767.49	7.903	0.7030	3926.53	6.715
1.3010	1.0737	3929.67	1745.149	1.2496	3927.6	14.939	0.8938	3933.41	9.042	3.9369	3945.54	1907.476	1.0976	3929.42	3.676
1.3979	1.1256	3929.62	16.102	1.2412	3927.92	12.995	1.0758	3935.24	6.406	0.8889	3928.67	6.87	2.8123	5816.27	22.597
1.4771	1.8625	4015.05	17.007	3.7480	4040.77	2293.994	1.9240	4017.84	7.383	1.9194	4018.25	5.545	1.2413	3930.14	4.913
1.5440	1.7971	4012.9	16.865	1.9021	4014.13	13.142	1.8400	4015.4	9.034	1.9480	4016.15	6.379	1.9175	4018.29	3.754
	Pt-Al^{3+}			Pt-Ga^{3+}			Pt-Cr^{3+}			Pt-Fe^{3+}			Pt-Mg^{2+}		
1.1761	1.2214	3764.23	22.838	0.6083	3926.05	17.776	1.4760	3767.37	26.675	0.3969	3925.49	8.2	0.3969	3925.49	8.2
1.3010	3.5944	3930.1	1.2214	0.5767	3925.9	16.375	0.2681	3926.38	9.775	3.5939	3925.48	7.887	3.5939	3925.48	7.887
1.3979	8.5010	7744.65	1935.273	1.0388	3936.28	15.786	1.0266	3944.92	9.343	0.9679	3938.03	6.593	0.9679	3938.03	6.593
1.4771	1.0571	3953.97	16.276	1.0714	3935.38	2473.38	0.8660	3940.57	6.893	0.9613	3941.18	5.341	0.9613	3941.18	5.341
1.5440	1.9590	4013.69	15.925	1.8880	4013.77	12.817	0.9216	3943.45	6.207	1.0004	3940.83	6.517	1.0004	3940.83	6.517

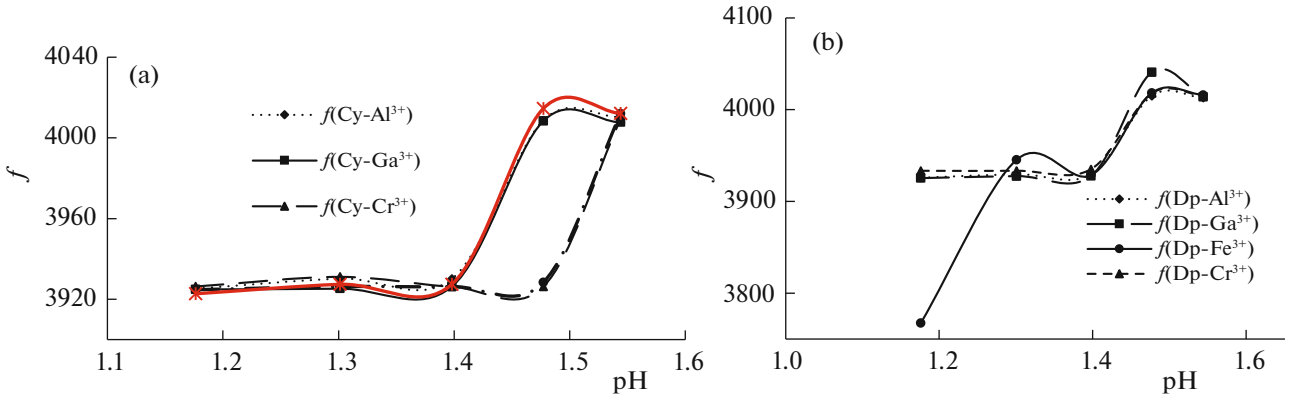

Fig. 4. (Color online) Changes of frequency (*f*) versus pH for (a) [Cy-Al^{3+}/Ga^{3+}/Cr^{3+}/Fe^{3+}/Mg^{2+}] chelation and (b) [Pt-Al^{3+}/Ga^{3+}/Cr^{3+}/Fe^{3+}] chelation in the weak acidic media by different concentrations of H^+ at 300 K.

tion were found to be significantly different with each metal treatment (Al^{3+}/Ga^{3+}/Cr^{3+}/Fe^{3+}/Mg^{2+}) (Table 4). It has been seen that by increasing the pH, the frequency of [ACN-Al^{3+}/Ga^{3+}/Cr^{3+}/Fe^{3+}/Mg^{2+}] chelation increases between pH ≈1.1–1.5 (Figs. 4a, 4b). The maximum frequency of Al^{3+} treated acylated Cy was greater indicating the development of bluer colors, especially in higher pH with effects on their visible light absorbance (Figs. 4a, 4b).

Although we have little information about the interaction of ACN with Cr^{3+}, it is trivalent M^{n+} having electrons in d orbitals, where addition of Cr^{3+} to the ACN of this study was also found to induce frequency and absorbance of spectra. In all pH, the mean frequency of the ACN of both sources was achieved to be various from one another with each metal cation. Similar trends occurred with Cr^{3+}, where the f_{max} of chelated Cy and Dp were greater while it has been indicated the larger f_{max} of the ACN with Cr^{3+} compared to Al^{3+}in chelation by Cy and Pt. Like Al^{3+}, the impacts of iron chelated to ACN were investigated to be better characterized to generate some ACN based blue colorations. Fe^{3+} is known to play an important role in many of the known pigment macromolecules [34]. Those metalloanthocyanins with Cy chromophores need Fe^{3+} to generate blue hues, but those based on Dp chromophores can proceed blue colors. So, it has been seen ACN formed bonds with Fe^{3+} producing the highest shifted of frequency and absorbance compared to other metalloanthocyanins (Figs. 3b and 4b).

As it has been seen in Table 4, the physical properties of high frequency and dipole moment for anthocyanin-metal cation chelation of Cy-Al^{3+}, Dp-Al^{3+}, and Pt-Al^{3+} have been calculated in weak acidic media extracted from the infrared computational method which shows a high deviation of absorbance for [Al^{3+}-chelation] of Dp pigment. The frequency achieved of IR vibrational spectra have shown that the normal mode of the active sites due to anthocyanin-metal cation chelation of Cy-Al^{3+}, Dp-Al^{3+}, and Pt-Al^{3+} in optimized weak acidic media approves the stability and color of these structures. The principal frequency vibrational modes have been illustrated based on the stability and color of various anthocyanin–metal cation chelation (Table 4).

In the next step, the atomic charge of indicated atoms in [ACN-Al^{3+}/Ga^{3+}/Cr^{3+}/Fe^{3+}/Mg^{2+}] chelation has been evaluated as the active parts of the molecules which play an important role for the electron charge transfer toward producing a range of various colors in water medium (Fig. 1 and Table 5).

In Figs. 5a–5e, it has been plotted the changes of atomic charge of labeled oxygen atoms and metal cations through optimized [ACN-Al^{3+}/Ga^{3+}/Cr^{3+}/Fe^{3+}/Mg^{2+}] chelation (Fig. 1); so, the results of Table 5 in a polar medium of water solution comparison to vacuum declare the stability and color of these compounds in the natural products of vegetables and fruits (Figs. 5a–5e).

The outlook of Fig. 5 recommends the reason for existing observed various results of [ACN-Al^{3+}/Ga^{3+}/Cr^{3+}/Fe^{3+}/Mg^{2+}] chelation which are principally linked to the position of active cites of labeled oxygen atoms and metal cations in these molecules which move the charge of electrons in aromatic cyclic chains because of water polar medium in contrast to vacuum and the lowest deviation for two media of water and vacuum has been indicated for ACN-Mg^{2+} (Fig. 5e).

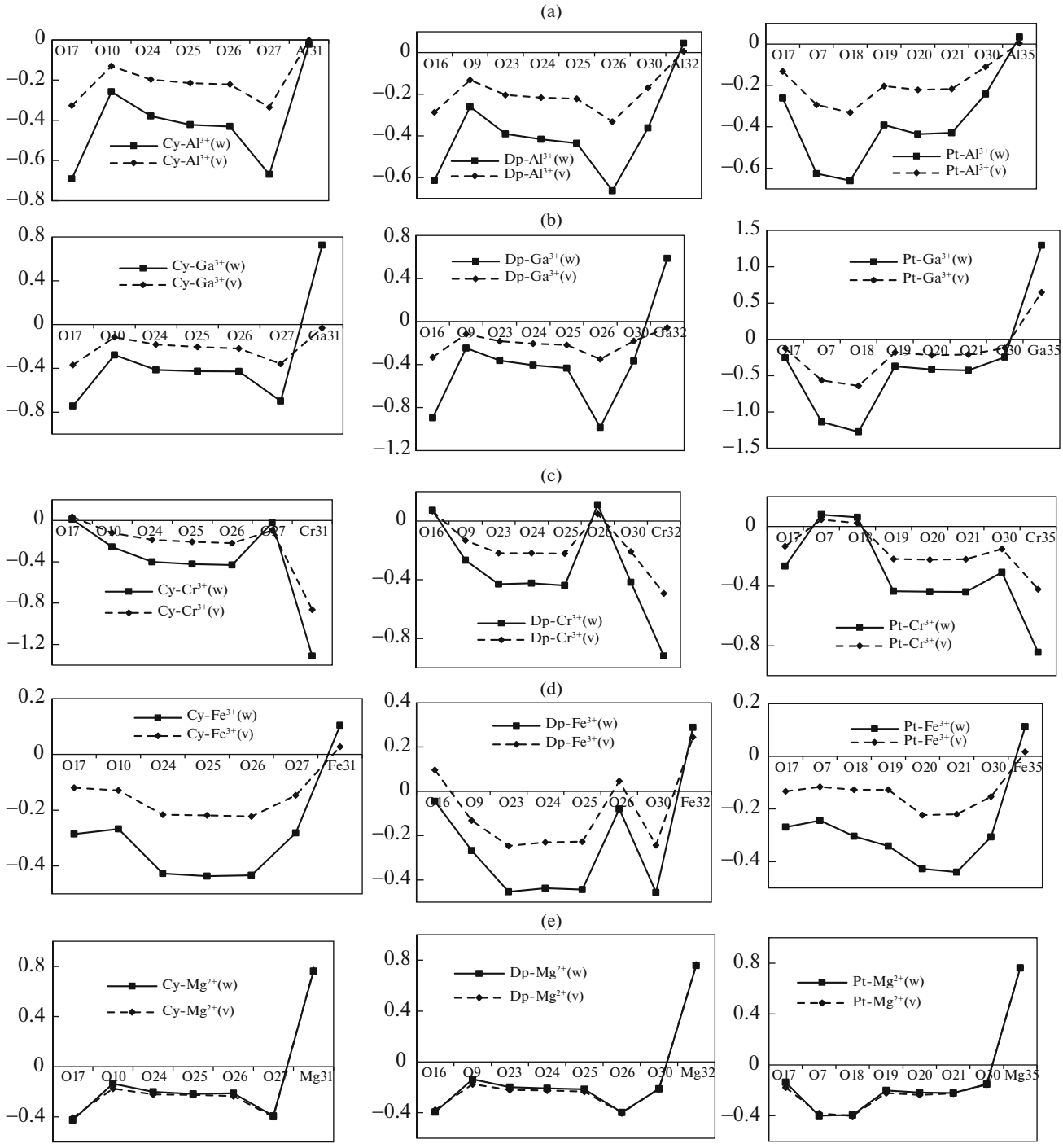

Fig. 5. Comparison of atomic charge versus labeled oxygen atoms and metal cations through optimized [ACN-Al^{3+}/Ga^{3+}/Cr^{3+}/Fe^{3+}/Mg^{2+}] chelation in vacuum and water media.

In fact, the spin density and partial charges have been obtained by fitting the electrostatic potential to fixed charge of O_{17}^{+}, O_{16}^{+}, and O_{7}^{+} cations for Cy-M^{n+} (31), Dp-M^{n+} (32), and Pt-M^{n+} (35), respectively (Table 5 and Fig. 5); therefore, the electrophilic groups of Cy, Dp anthocyanin pigments conduct us to find the reason for the activity and the stability of these structures in the natural products.

CONCLUSIONS

Generally, ACN is capable to chelate the M^{n+} through indicating the shift in their frequency and

Table 5. Atomic charge for oxygen atoms in molecules of [ACN-Al^{3+}/Ga^{3+}/Cr^{3+}/Fe^{3+}/Mg^{2+}-chelation] in different media of vacuum (v) and water (w)

Atom	ACN-Al^{3+} (v)	ACN-Al^{3+} (w)	ACN-Ga^{3+} (v)	ACN-Ga^{3+} (w)	ACN-Cr^{3+} (v)	ACN-Cr^{3+} (w)	ACN-Fe^{3+} (v)	ACN-Fe^{3+} (w)	CAN-Mg^{2+} (v)	ACN-Mg^{2+} (w)
ACN = Cy										
O10	−0.3274	−0.3639	−0.3685	−0.3752	0.0348	−0.0236	−0.1192	−0.1669	−0.4070	−0.4252
O+17	−0.1308	−0.1278	−0.1156	−0.1614	−0.1200	−0.1350	−0.1293	−0.1378	−0.1744	−0.1354
O24	−0.1977	−0.1818	−0.1823	−0.2314	−0.1866	−0.2141	−0.2164	−0.2108	−0.2217	−0.2014
O25	−0.2150	−0.2077	−0.2051	−0.2223	−0.2061	−0.2150	−0.2189	−0.2176	−0.2245	−0.2173
O26	−0.2213	−0.2094	−0.2185	−0.2093	−0.2187	−0.2125	−0.2224	−0.2112	−0.2350	−0.2123
O27	−0.3353	−0.3338	−0.3599	−0.3382	−0.0970	0.0752	−0.1466	−0.1350	−0.3996	−0.3935
M^{n+}31	−0.0025	−0.0201	−0.0315	0.7577	−0.8628	−0.4498	0.0273	0.0766	0.7701	0.7624
ACN = Dp										
O9	−0.2871	−0.3264	−0.3314	−0.5631	0.0678	0.0050	0.0968	−0.1422	−0.3774	−0.3932
O+16	−0.1314	−0.1285	−0.1163	−0.1313	−0.1319	−0.1350	−0.1311	−0.1362	−0.1753	−0.1361
O23	−0.2037	−0.1868	−0.1833	−0.1803	−0.2192	−0.2102	−0.2463	−0.2069	−0.2200	−0.1979
O24	−0.2165	−0.1995	−0.2054	−0.2018	−0.2185	−0.2054	−0.2302	−0.2071	−0.2242	−0.2074
O25	−0.2211	−0.2138	−0.2184	−0.2149	−0.2224	−0.2158	−0.2269	−0.2169	−0.2345	−0.2157
O26	−0.3313	−0.3316	−0.3504	−0.6333	0.0478	0.0634	0.0469	−0.1260	−0.4020	−0.3970
O30	−0.1690	−0.1922	−0.1812	−0.1867	−0.2076	−0.2105	−0.2433	−0.2131	−0.2124	−0.2107
M^{n+}32	0.0063	0.0385	−0.0575	0.6460	−0.4936	−0.4268	0.2444	0.0444	0.7645	0.7602
ACN = Pt										
O+7	−0.1322	−0.1285	−0.1249	−0.1317	−0.1324	−0.1329	−0.1327	−0.1367	−0.1762	−0.1361
O17	−0.2934	−0.3328	−0.5658	−0.5731	0.0460	0.0329	−0.1157	−0.1279	−0.3811	−0.3989
O18	−0.3315	−0.3287	−0.6413	−0.6332	0.0224	0.0389	−0.1271	−0.1769	−0.4015	−0.3940
O19	−0.2031	−0.1884	−0.1833	−0.1888	−0.2184	−0.2165	−0.1271	−0.2136	−0.2200	−0.2004
O20	−0.2211	−0.2146	−0.2203	−0.1940	−0.2228	−0.2152	−0.2230	−0.2039	−0.2345	−0.2168
O21	−0.2168	−0.2123	−0.2111	−0.2155	−0.2194	−0.2188	−0.2202	−0.2194	−0.2245	−0.2208
O30	−0.1100	−0.1314	−0.1202	−0.1263	−0.1503	−0.1565	−0.1532	−0.1529	−0.1520	−0.1505
M^{n+}35	0.0040	0.0304	0.6476	0.6472	−0.4207	−0.4231	0.0166	0.0958	0.7656	0.7630

absorbance spectra which are affected by several factors including the ACN structure, pH which is the important environmental factor in the expressed color of the solutions, and also the atomic configuration of the metallic cations. Divalent Mg^{2+} was found to impact ACN minimally with raising electron density in different pH; $Fe^{3+} \approx Ga^{3+} > Al^{3+} > Cr^{3+} \gg Mg^{n+}$. The color of the ACN chelates was discovered to be stable through the analysis and subsequent investigation considering stability that will be followed to estimate the efficiency of these types as food colorants.

Using Beer–Lambert law on [ACN-Al^{3+}/Ga^{3+}/Cr^{3+}/Fe^{3+}/Mg^{2+}] chelation of Cy, Dp, and Pt pigments by theoretical methods illustrates absorbance factor in vacuum and water media and then unravels the stabilization energy and geometry which have been impacted by IR theoretical modeling toward the thermodynamic properties and the electronic structural of optimized [ACN-Al^{3+}/Ga^{3+}/Cr^{3+}/Fe^{3+}/Mg^{2+}] com-

Table 6. Calculated thermochemical properties based on normal modes analyzing by m062x/cc-pvdz pseudo=lanl2 and Gaussian 2009 program package

Molecules	$E = E_0 + E_{vib} + E_{rot} + E_{trans}$	$H = E + RT$	$G = H - TS$
Cyanidin (Cy)	−7761.3389	−1156.0159	−227822.7071
Delphinidin (Dp)	−7853.3877	−1188.5057	−234587.2717
Petunidin (Pt)	−7690.8732	−1078.4232	−223041.8476

plexes resulting of metal chelation (Table 6). The results have exhibited that such extrapolation schemes significantly overestimate [ACN-Al^{3+}/Ga^{3+}/Cr^{3+}/Fe^{3+}/Mg^{2+}] chelation by sharp parts of electrophilic molecules in weak acidic media with different concentrations of H^+ which are the most active particles at the applied compounds in this project.

REFERENCES

1. F. H. Quina and E. L. Bastos, An. Acad. Bras. Cienc **90**, 681 (2018).
2. A. Castaneda-Ovando, M. L. Pacheco-Hernandez, M. E. Paez-Hernandez, Á. J. Rodriguez, and C. A. Galan-Vidal, Food Chem. **113**, 859 (2009).
3. F. Pina, J. Oliveira, and V. Freitas, Tetrahedron **71**, 3107 (2015).
4. A. Castañeda-Ovando, M. de Lourdes Pacheco-Hernández, E. Páez-Hernández, et al., Food Chem. **113**, 859 (2009).
5. N. P. Seeram, R. A. Momin, M. G. Nair, et al., Phytomedicine **8**, 362 (2001).
6. B. A. Cevallos- Casals and L.Cisneros- Zevallos, J. Agric. Food Chem. **51**, 3313 (2003).
7. Y. Katsumoto, M. Fukuchi-Mizutani, Y. Fukui, et al., Plant Cell Physiol. **48**, 1589 (2007).
8. A. Bąkowska-Barczak, Pol. J. Food Nutr. Sci. **14/55**, 107 (2005).
9. G. M. Robinson and R. Robinson, Biochem. J. **6**, 1647 (1932).
10. L. Jaakola, Trends Plant Sci. **18**, 477 (2013).
11. M. E. Olsson, K. E. Gustavsson, S. Andersson, A. Nilsson, and R. D. Duan, J. Agric. Food Chem. **52**, 7264 (2004).
12. H. A. Hassan and A. F. Abdel-Aziz, Food Chem. Toxicol. **48**, 1999 (2010).
13. B. Ghalandari, M. Monajjemi, and F. Mollaamin, J. Comput. Theor. Nanosci. **8**, 1212 (2011).
14. T. Ardalan, P. Ardalan, and M. Monajjemi, Fulleren. Nanotubes Carbon Nanostruct. **22**, 687 (2014).
15. L. P. Taylor and E. Grotewold, Curr. Opin. Plant Biol. **8**, 317 (2005).
16. W. A. Peer and A. S. Murphy, Trends Plant Sci. **12**, 556 (2007).
17. M. Monajjemi and M. Ahmadianarog, J. Comput. Theor. Nanosci. **11**, 1465 (2014).
18. E. A. Hudson, P. A. Dinh, T. Kokubun, M. S. Simmonds, and A. Gescher, Cancer Epidemiol. Biomark. Prevent. **9**, 1163 (2000).
19. J. B. Harborne, in *Phytochemical Methods, A Guide to Modern Techniques of Plant Analysis,* Ed. by J. B. Harborne, 3rd ed. (Chapman Hall, New York, 1998), p. 66.
20. M. Monajjemi, F. Mollaamin, M. R. Gholami, H. Yoosbashizadeh, S. K. Sadrnezhad, and H. Passdar, Main Group Metal Chem. **26**, 349 (2003).
21. F. J. Heredia, E. M. Francia-Aricha, J. C. Rivas-Gonzalo, I. M. Vicario, and C. Santos-Buelga, Food Chem. **63**, 491 (1998).
22. N. Ahmadiani, R. J. Robbins, T. M. Collins, et al., J. Agricult. Food Chem. **62**, 7524 (2014).
23. M. Monajjemi, L. Mahdavian, F. Mollaamin, and M. Khaleghian, Russ. J. Inorg. Chem. **54**, 1465 (2009).
24. E. M. Sarasia, S. Afsharnezhad, B. Honarparvar, F. Mollaamin, and M. Monajjemi, Phys. Chem. Liq. **49**, 561 (2011).
25. T. Borkowski, H. Szymusiak, A. Gliszczynska-Swiglo, and B. Tyrakowska, Food Res. Int. **38**, 1031 (2005).
26. A. A. Freitas, K. Shimizu, L. G. Dias, and F. H. Quina, J. Braz. Chem. Soc. **18**, 1537 (2007).
27. G. T. Sigurdson, P. Tang, and M. M. Giusti, Ann. Rev. Food Sci. Technol. **8**, 261 (2017).
28. A. A. Freitas, L. G. Dias, A. A. L. Maçanita, and F. H. Quina, J. Phys. Org. Chem. **24**, 1201 (2011).
29. A. Ananga, V. Georgiev, J. Ochieng, B. Phills, and V. Tsolova, in *The Mediterranean Genetic Code—Grapevine and Olive,* Ed. by D. Puljuha and B. Sladonja, 1st ed. (InTech, Rijeka, Croatia, 2013), p. 247.
30. S. Glińska, M. Bartczak, S. Oleksiak, A. Wolska, B. Gabara, M. Posmyk, and K. Janas, Ecotoxicol. Environ. Safety **68**, 343 (2007).
31. H. D. Schreiber, A. M. Swink, and T. D. Godsey, J. Inorg. Biochem. **104**, 732 (2010).
32. O. Dangles, M. Elhabiri, and R. Brouillard, J. Chem. Soc., Perkin Trans. **2**, 2587 (1994a).
33. M. Buchweitz, R. Carle, and D. R. Kammerer, Food Chem. **135**, 3010 (2012).
34. K. Yoshida, M. Mori, and T. Kondo, Nat. Product Rep. **26**, 884 (2009).
35. M. J. Frisch, G. W. Trucks, H. B. Schlegel, G. E. Scuseria, M. A. Robb, J. R. Cheeseman, G. Scalmani, V. Barone, B. Mennucci, G. A. Petersson, H. Nakatsuji, M. Caricato, X. Li, H. P. Hratchian, A. F. Izmaylov, et al., *Gaussian 09, Revision B.01* (Gaussian Inc., Wallingford, 2010).

36. F. Mollaamin and M. Monajjemi, J. Comput. Theor. Nanosci. **12**, 1030 (2015).
37. F. Wilfred, V. Gunsteren, and H. J. C. Berendsen, Angew. Chem., Int. Ed. Engl. **29**, 992 (1990).
38. W. Ni, G. Li, J. Zhao, J. Cui, R. Wang, Z. Gao, and Y. Liu, Infect Diseases (London) **50**, 507 (2018).
39. C. W. Andrews, J. Wisowaty, A. O. Davis, R. C. Crouch, and G. E. Martin, J. Heterocycl. Chem. **32**, 1011 (1995).
40. M. Monajjemi, B. Honarparvar, S. M. Nasseri, and M. Khaleghian, J. Struct. Chem. **50**, 67 (2009).
41. M. Monajjemi, R. Ghiasi, and M. A. Seyed Sadjadi, Appl. Organomet. Chem. **17**, 635 (2003).
42. G. Cohen and H. Eisenberg, Biopolymers **6**, 1077 (1968).
43. P. Beak, J. B. Covington, S. G. Smith, J. M. White, and J. M. Zeiger, J. Org. Chem. **45**, 1354 (1980).
44. J. G. Kirkwood, J. Chem. Phys. **2**, 767 (1934).
45. J. G. Kirkwood, J. Chem. Phys. **7**, 911 (1939).
46. L. Onsager, J. Am. Chem. Soc. **58**, 1486 (1936).
47. M. A. Wong, M. J. Frisch, and K. B. Wiberg, J. Am. Chem. Soc. **113**, 4776 (1991).
48. M. A. Wong, M. J. Frisch, and K. B. Wiberg, J. Am. Chem. Soc. **114**, 523 (1992)
49. V. S. Lee, P. Nimmanpipug, F. Mollaamin, S. Thanasanvorakun, and M. Monajjemi, Russ. J. Phys. Chem. A **83**, 2288 (2009).
50. M. Monajjemi, N. Farahani, and F. Mollaamin, Phys. Chem. Liq. **50**, 161 (2012).
51. S. Kunsági-Máté, E. Ortmann, L. Kollár, K. Szabó, and M. P. Nikfardjam, J. Mol. Struct. **891**, 471 (2008).
52. L. Estévez, N. Otero, and R. a. Mosquera, Theor. Chem. Acc. **128**, 485 (2011).
53. R. P. Mason, in *Trace Metals in Aquatic Systems,* Ed. by R. P. Mason, 1st ed. (Blackwell, Wiley, Chichester, West Sussex, U.K., 2013), p. 49.